RESEARCH ARTICLE

Macromolecular Materials and Engineering
Open Access
www.mame-journal.de

An Adaptive Artificial Neural Network Model for Predicting Friction and Wear in Polymer Matrix Composites: Integrating Kragelsky and Archard Laws

*Ravisrini Jayasinghe, Maximiano Ramos, Ashveen Nand, and Maziar Ramezani**

This study presents a hybrid modeling approach that integrates Kragelsky's friction law and Archard's wear law with an artificial neural network (ANN) to predict the coefficient of friction (COF) and specific wear rate (SWR) in epoxy-based self-lubricating composites reinforced with graphite and MoS_2. Given the complex, nonlinear interactions among tribological parameters such as contact pressure, sliding speed, hardness, and filler composition, traditional empirical models often fail to capture wear behavior accurately. The proposed ANN architecture comprises an input layer, three hidden layers employing sigmoid, ReLU, and power activation functions, and an output layer predicting COF and SWR. The network is trained using a feed-forward method with backpropagation to minimize prediction error. SEM analysis reveals that graphite imparts superior wear resistance compared to MoS_2. The ANN achieved significantly higher prediction accuracy for graphite-reinforced composites. For COF, graphite yielded an MSE of 0.00073 and R^2 of 0.9047, while MoS_2 showed an MSE of 0.00318 and R^2 of 0.5567. For SWR, graphite attained an MSE of 1.3351 and R^2 of 0.9809, compared to MoS_2 with an MSE of 1.6993 and R^2 of 0.8271. The reduced performance in MoS_2 predictions is attributed to its oxidative degradation forming MoO_3. The model also offers 3D surface simulations, aiding in composite design optimization and reducing experimental costs.

1. Introduction

Tribology, the science of friction, wear, and lubrication, has garnered significant attention due to the increasing demand for advanced materials in mechanical systems. Understanding friction and wear under diverse operating conditions, along with their dependencies, is critical for enhancing system performance and reducing energy losses throughout the lifecycle of mechanical components.[1–5] In literature, various methods are typically mentioned, but ANNs remain the most prominent and effective over other methods due to their ability to predict the behavior of wear and friction in complex systems.[2,6 7]

Other soft computing approaches, such as genetic algorithms,[8] particle swarm optimization,[8–10] and response surface methodology,[8,9,11,12] have also been widely utilized in various optimization and predictive modeling tasks. Genetic algorithms are particularly effective for solving complex, non-linear optimization problems by mimicking the process of natural selection to find optimal or near-optimal solutions. Particle swarm optimization, inspired by the social behavior of birds and fish, is a robust technique for exploring large search spaces efficiently, while response surface methodology is commonly employed for modeling and analyzing the influence of multiple variables to optimize desired outcomes.[13] ANNs offer a clear advantage by capturing relationships between variables such as material, test conditions, and environmental factors without requiring explicit mathematical models for nonlinear interactions. Recent studies further demonstrate that ANNs significantly enhance the accuracy of conventional predictive models, offering a powerful approach to improving predictive capabilities.[14]

Traditional theoretical models frequently fail to capture nonlinear correlations between these variables. The ability of ANNs to simulate complex systems without the requirement for explicit mathematical formulations is one of their main advantages.[15] Early-stage research has shown that artificial neural networks have the capability to forecast wear rate in mechanical systems across different load and sliding speed conditions.[7] Similarly, studies have demonstrated that ANN models can accurately forecast friction coefficients in sliding contact situations, surpassing traditional regression models.[14,16] ANNs have been utilized in a range of tribological scenarios, such as predicting wear in polymers,[17] studying friction in lubricated contacts,[18] and

R. Jayasinghe, M. Ramos, M. Ramezani
Department of Mechanical Engineering
Auckland University of Technology
Auckland 1010, New Zealand
E-mail: maziar.ramezani@aut.ac.nz

A. Nand
Faculty of Engineering
University of Auckland
Auckland 1010, New Zealand

The ORCID identification number(s) for the author(s) of this article can be found under https://doi.org/10.1002/mame.70004

DOI: 10.1002/mame.70004

simulating the wear rate of polymers during dry sliding.[19,20] ANN models have also been employed to predict wear in metal cutting operations, considering tool geometry, material, and operational factors[20,21] More recent studies have focused on improving the accuracy and robustness of ANN models in tribology, developing ANN-based models that integrate various environmental factors, including temperature and humidity, to predict the wear of steel components.[22] Further advances have incorporated hybrid ANN models, combining traditional empirical models with neural networks for enhanced predictive power.[23,24] ANNs have also been utilized in lubricated systems to enhance lubrication strategies and reduce energy waste,[24] as well as to optimize lubrication parameters in journal bearings. Additionally, ANNs have been employed to predict wear in automotive parts under mixed lubrication scenarios.[25] Employing ANNs in tribological applications has proven successful in enhancing the precision of forecasts concerning friction and wear, showing substantial promise for improving the functionality and design of mechanical systems.[20,21]

Epoxy polymers have good mechanical strength, strong adhesion, and chemical resistance, which make them suitable for a wide range of engineering applications. However, pure epoxy materials exhibit poor tribological qualities, including high friction, low wear resistance, and non-recyclable waste at the end of the life cycle, despite these benefits. Innovative recyclable materials are still under development, mainly to replace lightweight,[26,27] high-strength epoxy. Literature studies show that surface texturing significantly influences the tribomechanical properties of epoxy composites reinforced with chemically activated carbon derived from palm kernel shells (PKSAC) and coconut shells (CSAC). Research utilizing Box-Behnken design to analyze the effects of varying compositions, particle sizes, and reinforcement amounts has demonstrated that surface texturing generally reduces mechanical strength, but effectively decreases wear rate and increases the coefficient of friction.[27] Another study shows that incorporating natural fillers derived from agricultural waste, such as Bagasse Ash (BA) and Pistachio Shell Ash (PA), into epoxy composites can enhance mechanical properties while promoting environmental sustainability.[28] Also, palm kernel shell-derived $CaCO_3$ fillers can enhance the tensile and wear properties of epoxy composites due to strong filler-matrix bonding.[29] Natural fibers and particulates are increasingly favored over synthetic fibers in polymer composites due to their eco-friendliness, abundance, and cost-effectiveness. Further research examining the erosive wear behavior of epoxy composites reinforced with bio-waste (orange peel) indicates that impact velocity and impingement angles significantly affect erosion rates, with tests conducted using silica sand as the erodent.[30] These findings suggest that surface texturing can be a viable strategy to enhance the performance of recyclable polymer composites for automotive applications, despite the reduction in mechanical strength.

In tribological applications, epoxy often undergoes rapid surface degradation upon sliding or rotating motion, which can result in material failure.[31] This limitation restricts epoxy's suitability in applications where wear and friction are major concerns, particularly in moving mechanical parts. To overcome these limitations, researchers have focused on enhancing epoxy's tribological performance by adding solid lubricants such as graphite and MoS_2.[31,32] Graphite and MoS_2 are both widely recognized for their exceptional lubricating properties, which reduce friction and wear. The resulting self-lubricating composite produced by dispersing these materials into the epoxy matrix significantly improves the durability and reliability of epoxy-based components. Even in harsh working conditions, these solid lubricants reduce friction by forming a sliding interface that minimizes wear and enhances material longevity.[33] Friction and wear properties in polymers are challenging to predict due to the complex nature of tribological interactions, material viscoelasticity, temperature sensitivity, and surface film formation. Additional complexities arise due to material heterogeneity from reinforcements, nonlinear behavior, and environmental factors. These dynamic and interdependent variables necessitate advanced techniques, such as ANN, for accurately predicting the tribological performance of polymer composites.[34,35]

The novelty of this research lies in its dual-output predictive approach using an ANN integrated with Kragelsky's friction law and Archard's wear law. Although previous studies have used Kragelsky's friction model in conjunction with ANNs to predict wear rates, the current research uniquely extends this approach to simultaneously predict both COF and specific wear rate while keeping the contact pressure, sliding speed, hardness, and material composition as input parameters. While traditionally applied to wear rate analysis, Kragelsky's friction law provides a comprehensive basis for understanding frictional interactions in polymer-based composites. In this study, Kragelsky's friction law is applied to epoxy composites reinforced with graphite and MoS_2 to demonstrate its adaptability and relevance to polymer systems, where frictional behavior may be influenced by complex tribological interactions. The ANN with multiple hidden layers captures the nonlinear relationships among tribological inputs, including material properties, pressure, and velocity. This integrated model is expected to improve not only predictive accuracy but also to streamline the optimization of composite formulations, reducing both experimental efforts and associated costs. This study thus represents a significant advancement in tribological modeling, providing a robust framework for predicting friction and wear parameters in epoxy-based composites.

2. Experimental Section

2.1. Materials and Sample Preparation

For this study, bisphenol A/epichlorohydrin epoxy resin (50-70 wt%) and isophoronediamine (3-aminomethyl-3,5,5-trimethylcyclohexylamine) curing agent (50–60 wt%) were sourced from Norski (Plimmerton, New Zealand. The mold release agent was also obtained from the same supplier. Molybdenum(IV) sulfide (MoS_2), with a grain size <2 μm and purity >98%, was acquired from AK Scientific (San Francisco, California). Graphite powder, with a particle size of $d \approx 2.5$ μm and impurities <0.003%, was obtained from Final Advanced Materials (Didenheim, France) and used as a solid lubricant.

2.2. Sample Preparation

The MoS_2/epoxy and graphite/epoxy composites were manufactured using an open-mold technique, with epoxy serving as the

Table 1. Test matrix.

Load [N]	Frequency [Hz]	Composition [wt%] (graphite and MoS_2)	Replicates
10	2, 5, 8	0.1, 0.2, 0.3, 0.4, 0.5	3
5, 10, 15	5	0.1, 0.2, 0.3, 0.4, 0.5	3

matrix and MoS_2 and graphite as self-lubricating fillers. To ensure consistency and uniformity, rigorous precautions were followed during the mixing process. Ultralow amounts of MoS_2 and graphite were used following the literature as it was observed that ultra-low concentrations improved exfoliation and optimized mechanical and thermal properties of epoxy matrix.[36–38] The synergistic effect of MoS_2 and graphite was not considered; instead, their individual lubricating effects were examined by incorporating MoS_2 and graphite powders into the epoxy resin at mass fractions of 0.1, 0.2, 0.3, 0.4, and 0.5 wt% (appendix 1 experimental design give the further details).

The composite mixtures were initially stirred for 1 h to achieve homogeneity, followed by high-intensity ultrasonication (nominal power: 550 W, frequency: 20 kHz) for 20 min to ensure thorough dispersion. Ultrasonication was performed with the beaker submerged in an ice-water bath to prevent heat accumulation. The curing agent (isophoronediamine) was added at a 4:1 ratio (epoxy: hardener) by weight at room temperature. After mixing thoroughly, the composites were degassed under -1 bar pressure for 10 min to remove trapped air. The degassed mixtures were poured into prepared aluminum molds, which were presmoothened with a Scotch-Brite pad and treated with mold release agent.

Curing conditions followed supplier guidelines, initially cured overnight at 10 °C, followed by post-curing at 60 °C to ensure maximum composite strength. A reference sample (pure epoxy without fillers) was also prepared to serve as a baseline for assessing the impact of the MoS_2 and graphite additives on tribological properties.

2.3. Tribological Characterization

The epoxy composite samples were tested on a linear reciprocating tribometer to train the ANN. Tribometer parameters, derived from literature on polymer bearing applications, were optimized to include loads from 5 to 15 N (maximum contact pressures: 80–130 MPa) and sliding frequencies of 2–8 Hz.[3,39,40] These parameters were chosen to simulate typical operational conditions of polymer composites.

The test variables consisted of three applied loads: 5, 10, and 15 N; five filler compositions: 0.1, 0.2, 0.3, 0.4, and 0.5 wt%; and three sliding frequencies: 2, 5, and 8 Hz. These sliding frequencies corresponded to sliding speeds of 0.02, 0.07, and 0.2 m s^{-1}, respectively. The test plan was divided into two main configurations, as shown in **Table 1**, to examine the impact of sliding speed on the tribological properties at a constant load of 10N, and the effect of varying load (5, 10, and 15 N) at a constant sliding frequency of 5 Hz. Each test run recorded the COF and specific wear rate (mm^3/Nm) as the primary outputs.

For the friction tests, a chromium steel ball (counterpart) with a radius of 5 mm, hardness of RHC 50–55, and surface roughness of $Ra \approx 2.5$ µm was used. An Rtec tribometer MFT-5000 (Rtec Instruments, USA) was employed to perform the sliding wear tests. Dry sliding was conducted under a constant temperature of 22 °C and a relative humidity of 60%. To ensure accuracy and repeatability, each experimental condition was repeated three times. During the testing process, a dwell time of 0.2 s was used to collect COF data, and the curve was smoothed to improve accuracy. The steady-state COF was identified by monitoring the COF curve until it reached a stable, consistent pattern, which typically occurred after approximately 10 min of testing. Once the COF values stabilized, the average COF was calculated over this steady-state interval. To obtain the representative COF for each test run, the total mean value from the steady-state period was used. The wear values reported in this study are the total wear values measured at the end of each test. This approach ensures consistent and accurate evaluation of the wear performance for all tested samples under the specified test conditions. Each test condition was repeated three times to ensure reliable average COF values, with standard errors included to enhance the precision and consistency of the results.

The specific wear rate was calculated using the previously reported equation.[41–43] The wear volume of the samples was measured using a surface profilometer (Taylor Hobson Form Talysurf 50) equipped with a diamond stylus (4 µm diameter). The total sliding distance was fixed at 400 m, with the wear track width maintained at 7 mm. Profilometer readings were processed in MATLAB to extract the surface track depth, width, and radius, which were used to calculate the worn surface volume. To determine hardness, a durometer type D was used in accordance with ASTM D2240. The average values were calculated for each set of five samples by performing two repeated measurements per experiment condition, as referenced in.[44]

The maximum contact pressure was calculated using the Hertz ball on flat contact theory according to the previously reported method[45] for each test. Tribology extensively uses this theory to simulate the contact mechanics between two elastic bodies under load. Hertz theory presupposes that the materials are homogeneous and isotropic. The maximum contact pressure for two in-contact spherical surfaces was determined by taking the contact radius and the applied normal load and the Young's modulus of the ball (chromium steel) and the composite (epoxy) and their Poisson's ratios . High Young's modulus (200 GPa) and low Poisson's ratio (around 0.3) are typical characteristics of chromium steel.[46] The Young's modulus of Epoxy Composite is substantially lower (usually between 2 and 5 GPa) and its Poisson's ratio is greater (0.35).[47] The resultant Maximum contact pressure values are mentioned in Appendix 1.

3. Predictive Model

3.1. Kragelsky and Archard Laws

Wear behavior is characterized by wear volume (w), representing material loss due to wear. Wear is an inherently irreversible process involving material removal, and wear values are strictly non-negative. Wear volume loss is related to the applied normal load

F via the formula $P = F/A$, where A denotes the apparent contact area. The average wear depth, or linear wear, is calculated as w/A.

The Archard-Kragelsky wear law—a hybrid model—integrates fundamental tribology theories to describe wear between contact surfaces. Archard's wear equation, shown below in Equation (1), states that the wear volume w is directly proportional to the normal load F, sliding distance L, and inversely proportional to material hardness H[48,49]:

$$W = \frac{KFL}{H} \tag{1}$$

To account for the nonlinear relationship of wear rate with influencing factors like normal pressure p and sliding velocity v, Equation (1) can be generalized into a nonlinear form in Equation (2)[50]:

$$W = K_w \left(\frac{P}{P_c}\right)^{\alpha} \left(\frac{V}{V_c}\right)^{\beta} \tag{2}$$

where P_c and V_c are characteristic values of contact pressure and sliding velocity correspondingly, and K_w is the dimensional wear coefficient. The exponents α and β are empirical constants determined through experimental data via nonlinear regression.[51–53] This equation can be extended to include other physical and material parameters such as hardness (H) and composition (C),[54] as in Equation (3):

$$W = K_w f\left(\frac{P}{P_C}, \frac{V}{V_C}, \frac{H}{H_C}, \frac{C}{C_C}, \ldots.\right) \tag{3}$$

where H_c and Cc are characteristic values for hardness and composition, respectively, yielding a more complete model by including variables critical to wear, enhancing predictive accuracy. To model K_w with ANN, Equation (4) is written:

$$W = K_{wANN}\left(\frac{P}{P_C}\right), \left(\frac{V}{V_C}\right), \left(\frac{H}{H_C}\right), \left(\frac{C}{C_C}\right) \tag{4}$$

where K_w is expressed as a function of pressure P, velocity V, and the physical properties of the materials in contact, composition, C and hardness H. This complex interaction is modeled using a four-layer feed-forward back-propagation ANN.

3.2. Artificial Nural Network Architecture

The proposed ANN architecture has an input layer for the variables P (pressure), V (velocity), C (composition of MoS_2 and graphite), and H (hardness), forming an input vector:

$$X = [P, V, C, H]^T \tag{5}$$

The developed ANN has a four-layer structure; the first hidden layer consists of 30 neurons having a sigmoid activation function. The second hidden layer consists of 20 neurons with a linear activation function. The third hidden layer is composed of 15 neurons with a power activation function to capture the nonlinearity of wear behavior. The output layer provides the predicted values for K_{wANN} (P, V, C, H), specific wear rate, and coefficient of friction.

The input vector X is processed through the network with weights w and biases b. For each neuron in the first hidden layer, sigmoid activation is used, with the input multiplied by the weights and added to the bias. The activation function receives input from each neuron (i):

$$z_1 = w_1^T X + b_1 \tag{6}$$

The output of each neuron is calculated using the sigmoid activation function.

$$a_1 = \sigma\, z_1 = \frac{1}{1 + e^{-z_1}} \tag{7}$$

Second, the hidden layer uses a linear activation function.

$$z_2 = w_2^T a_1 + b_2 \tag{8}$$

This layer directly passes the weighted sum of inputs to the next layer without nonlinearity.

$$a_2 = z_2 \tag{9}$$

The third hidden layer applies a power activation function to introduce nonlinearity:

$$z_3 = w_3^T A_2 + b_3 \tag{10}$$

A power activation function will transform the output:

$$a_3 = z_3^n \tag{11}$$

The exponent n is determined empirically to optimize the model's performance. This nonlinearity allows the network to capture complex relationships between inputs and outputs better.

The output layer of the ANN provides predictions for the wear factor (K_wANN), specific wear rate (SWR), and COF. Specific wear rate (SWR) is predicted using the function (K_wANN), which depends on parameters including pressure (P), velocity (V), hardness (H), and composition (C):

$$\text{SWR} = K_{wANN}\,(P, V, H, C) \tag{12}$$

COF is determined using the output of the third hidden layer (A_3):

$$\text{COF} = [w_4^T A_3 + b_4] \tag{13}$$

Here, w_4 represents the weights connecting the third hidden layer to the output layer, and b_4 is the bias term for the output layer.

Training the ANN requires a loss function and validation of the prediction accuracy.[24,34]

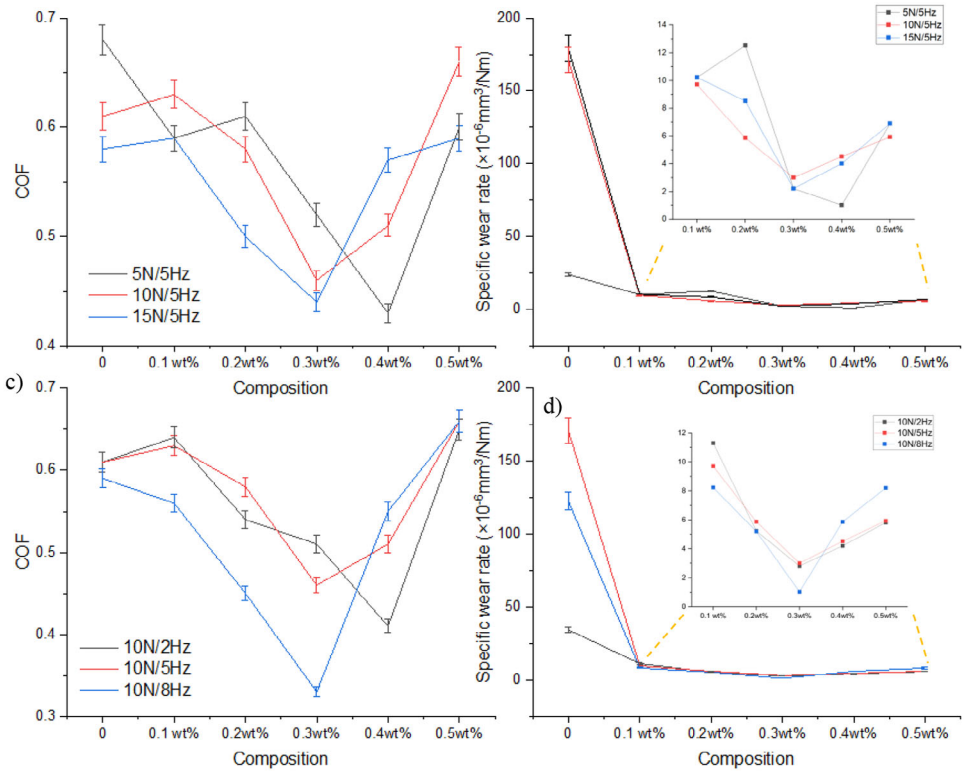

Figure 1. Graphite composition (wt%) versus a) COF and; b) specific wear rate at a constant frequency of 5 Hz under different loads (5, 10, and 15 N), graphite composition (wt%) versus c) COF and; d) specific wear rate at a constant load (10 N) under different frequencies (2, 5, and 8 Hz).

3.2.1. Loss and Optimization

The ANN is trained by minimizing the mean squared error between predicted and actual values for both the SWR and COF:

$$\text{Loss} = \frac{1}{N}\sum_{i=1}^{N}\left(\left(\text{SWR}_{\text{pred},i} - \text{SWR}_{\text{true},i}\right)^2 + \left(\text{COF}_{\text{pred},i} - \text{COF}_{\text{true},i}\right)^2\right) \tag{14}$$

where N represents the number of training samples, which was 50, SWR_{pred} and COF_{pred} are the ANN predicted values, and SWR_{true} and COF_{true} are the actual experimental values.

The backpropagation technique is used to minimize the loss function. It improves and adjusts the weight and biases using gradients computed with the assistance of the chain rule.

The updated rules for weights w_{ij}^{l} and biases b_{i}^{l} at layer l can be expressed as;

$$w_{ij}^{l} \leftarrow w_{ij}^{l} - \eta\frac{\partial \text{Loss}}{\partial w_{ij}^{l}} \quad \text{and} \quad b_{i}^{l} \leftarrow b_{i}^{l} - \eta\frac{\partial \text{Loss}}{\partial b_{j}^{l}} \tag{15}$$

where η is the learning rate, this technique could hybrid classical tribological formulae with machine learning techniques in a way that predicted specific wear rate as well as COF variation under different conditions, hence being of considerable importance in optimizing material performance during tribological applications.

4. Results and Discussions

4.1. Tribological Properties

Figure 1 illustrates the tribological performance of Graphite-reinforced epoxy composites under varying loads and sliding frequencies, demonstrating a significant improvement in both the coefficient of friction (COF) and specific wear rate with increasing graphite composition up to 0.3 wt%. At a constant frequency of 5 Hz, the COF shows a decreasing trend as the load increases from 5 to 15 N, indicating enhanced lubrication effectiveness at higher loads, particularly at 0.3 wt%. However, further increasing the graphite content to 0.5 wt% leads to an increase in COF, likely due to graphite particle agglomeration, which disrupts uniform tribofilm formation and hinders its lubricating ability. The addition of graphite within the range of 0.1 wt% to 0.3 wt% significantly reduces the COF due to the formation of a continuous and uniform tribofilm on the contact surface, facilitating easy shear between the sliding surfaces. However, when the graphite concentration exceeds 0.3 wt%, particle agglomeration becomes a critical issue, leading to the formation of clusters rather than a well-distributed lubricating layer. These clusters can act as abrasive particles, diminishing the lubrication efficiency and resulting in increased COF and wear rate.

The specific wear rate shows a drastic reduction from 0 to 0.1 wt%, followed by a near-constant value for higher compositions, suggesting that even a small amount of graphite provides substantial wear protection. Compared to the neat epoxy, the wear resistance after 0.1 wt% graphite addition is very im-

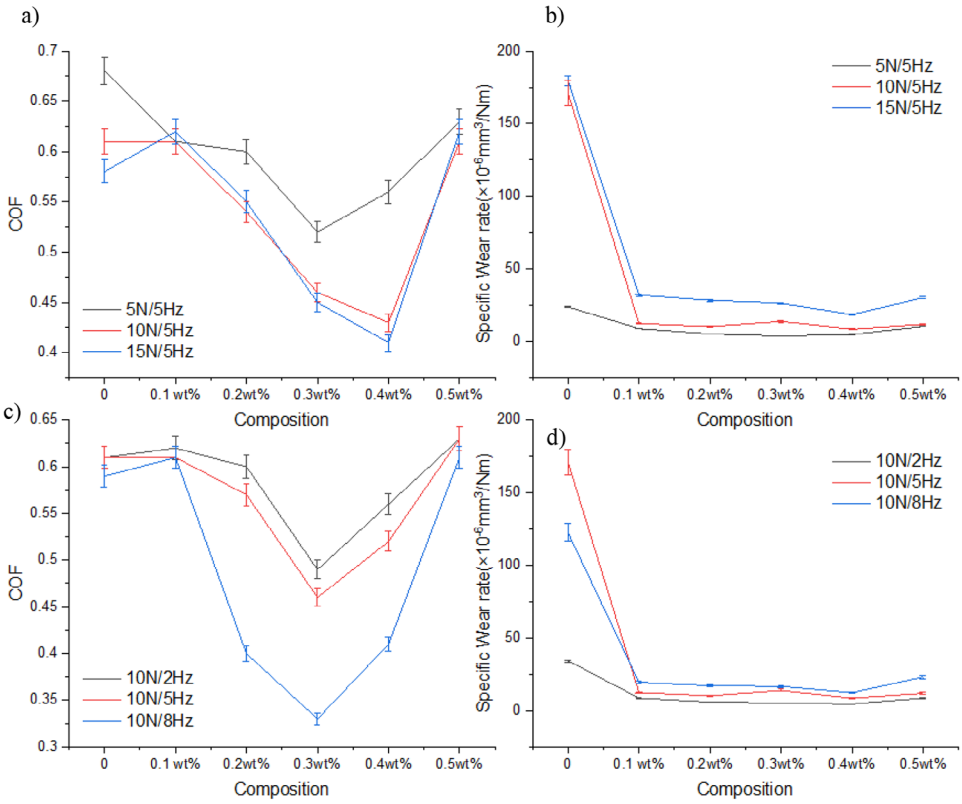

Figure 2. MoS_2 composition (wt%) versus a) COF and; b) specific wear rate at a constant frequency of 5 Hz under different loads (5, 10, and 15 N), MoS2 composition (wt%) versus c) COF and; d) specific wear rate at a constant load (10 N) of under different frequencies (2, 5, and 8 Hz).

pressive, with a drastic decrease in specific wear rate, as clearly shown in Figure 1b,d. Additional graphite beyond 0.1 wt% continues to maintain superior wear resistance, indicating that the incorporation of graphite effectively contributes to the formation of a protective tribofilm, preventing direct contact between the epoxy matrix and the steel counterpart.

When evaluated at a constant load of 10 N under varying frequencies (2, 5, and 8 Hz), the COF decreases notably with increasing frequency, with the lowest COF observed at 0.3 wt% graphite composition under 8 Hz. This trend is attributed to enhanced exfoliation and better dispersion of graphite particles at higher frequencies, which promote the formation of a lubricating tribofilm. Correspondingly, the specific wear rate also decreases with increasing frequency, with noticeable improvement at 0.1 wt%. These findings confirm that the optimal graphite composition for superior tribological performance is 0.3 wt%, where the COF reaches its minimum, and the specific wear rate stabilizes effectively. Additionally, the results emphasize the critical role of frequency in enhancing lubrication by assisting in the dispersion and incorporation of graphite into the protective tribofilm.

Figure 2 demonstrates the tribological performance of MoS_2-reinforced epoxy composites under varying loads and sliding frequencies, following a pattern similar to graphite due to its layered crystal structure and ability to form a lubricating tribofilm. The coefficient of friction (COF) decreases with increasing MoS_2 composition up to 0.3 wt% for all applied loads and frequencies. This reduction is attributed to the lamellar structure of MoS_2, where weak van der Waals forces between layers allow easy shear during sliding, promoting effective lubrication. Notably, the lowest COF is observed at 0.3 wt% across all loads and frequencies, with the most significant reduction achieved at 15 N load and 8 Hz frequency, respectively. However, beyond 0.3 wt%, the COF increases due to agglomeration of MoS_2 particles, which disrupts uniform dispersion and tribofilm formation, resulting in uneven sliding and increased friction. The specific wear rate exhibits a drastic reduction from 0 to 0.1 wt%, followed by a near-constant value for higher compositions, indicating that even a small amount of MoS_2 effectively enhances wear resistance. This improvement is due to the formation of a protective MoS_2 tribofilm that prevents direct contact between the epoxy matrix and the steel counterpart. However, at higher MoS_2 concentrations (0.4 wt% and 0.5 wt%), particle agglomeration leads to localized abrasive wear, slightly increasing the wear rate. Additionally, higher frequencies (8 Hz) promote better exfoliation and dispersion of MoS_2 particles, resulting in enhanced tribofilm formation and lower COF and wear rates. These findings confirm that the optimal MoS_2 composition for superior tribological performance is 0.3 wt%, where the COF reaches its minimum, and the wear rate stabilizes effectively. The similarities in the tribological behavior of MoS_2 and Graphite are evident, as both materials exhibit layered structures that promote lubrication and a tendency for agglomeration at higher compositions, reducing their effectiveness.

Figure 3 illustrates the variation of the COF against time for neat epoxy, 0.3 wt% graphite/epoxy, and 0.3 wt% MoS_2/epoxy composites. The neat epoxy shows the highest COF, starting

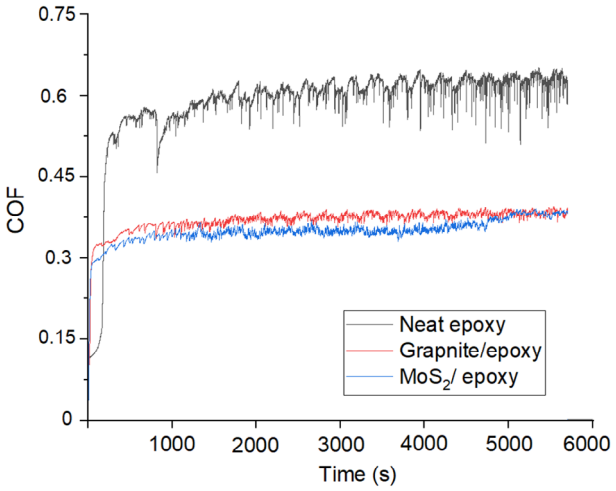

Figure 3. COF versus time graph for the neat epoxy, 0.3 wt% graphite/epoxy and 0.3 wt% MoS_2/ epoxy after 400 m sliding length under 8 Hz frequency and 10 N load.

from a sharp rise and stabilizing around 0.6. The variation in the CF of neat epoxy is significantly high due to abrasive wear conditions, resulting from poor lubrication and higher frictional forces during sliding. The 0.3 wt% graphite/epoxy composite displays a moderate reduction in COF, stabilizing around 0.3 to 0.35, indicating the lubricating effect of graphite. The 0.3 wt% MoS_2/epoxy composite follows the same pattern of COF variation and stabilizing around 0.3, suggesting better lubrication and lower friction compared to both neat epoxy and Graphite/epoxy. The stabilized regions for all samples indicate the achievement of a steady-state condition after the initial running-in phase. This comparison confirms the effectiveness of MoS_2 and graphite as solid lubricants in reducing friction compared to neat epoxy.

Figure 4 provides SEM images of the wear track on a 0.3 wt% graphite/epoxy composite after 400 m of sliding under various loading and frequency conditions, shown at two magnifications (Figure 4a,b), taken at 10 N and 2 Hz, exhibit significant wear features, including wear debris, delamination, and prominent cracks. Higher magnification reveals smaller cracks, indicating early crack propagation. Figure 4c,d, taken at 5 N and 5 Hz, show fatigue cracks and wear debris, highlighting surface damage and subsurface fatigue as dominant wear mechanisms. Figure 4e,f, under 10N and 5 Hz, show delamination and abrasive wear grooves, with small cracks observed at higher magnification, suggesting the onset of abrasive wear due to increased load. Figure 4g,h, at 10 N and 8 Hz, display fatigue cracks and abrasive grooves, with visible wear debris, indicating intensified abrasive wear at higher frequencies. Figure 4i,j, at 15 N and 5 Hz, reveal severe delamination and abrasive wear, with cracks filled with wear debris, suggesting crack propagation and particle embedment as primary wear mechanisms under high load conditions.

Figure 5 presents SEM images of the wear track on a 0.3 wt% MoS_2/epoxy composite after 400 meters of sliding under different loads and frequencies, with close-ups at higher magnification. Figure 5a,b, at 10 N and 2 Hz, show extensive wear features such as delamination and wide cracks. The significant cracking suggests severe wear at low frequency, which limits effective removal of MoS_2 from the surface. Figure 5c,d, at 5 N and 5 Hz, shows moderate delamination and fewer cracks, indicating reduced wear severity under these milder conditions. Figure 5e,f, at 10 N and 8 Hz, reveals relatively low wear compared to other conditions, with increased frequency aiding in the removal of the MoS_2 layer, thus reducing friction and wear. Crack initiation is observed, but the wear track is smoother with minimal delamination. Figure 5g,h, at 10 N and 5 Hz, exhibits significant material removal and wide cracks. Figure 5i,j, at 15 N and 5 Hz, reveal severe material removal with cracks filled with wear debris, indicating high wear intensity at increased load. The accumulation of wear debris within cracks suggests that under high load, MoS_2 is less effective in protecting the surface, leading to extensive wear and crack propagation.

SEM observations indicate that graphite provides superior wear resistance compared to MoS_2 in epoxy composites. Although differences in wear performance between graphite and MoS_2 may not be evident in COF and specific wear rate measurements alone, SEM images show visibly less surface damage in graphite-reinforced composites in their microscale. This suggests that graphite offers better protection against wear under sliding conditions. In contrast, MoS_2 may undergo oxidative degradation in atmospheric conditions, forming MoO_3 upon exposure to oxygen and elevated temperatures. This oxide layer diminishes MoS_2's lubrication properties, reducing its wear resistance.[55] Consequently, graphite proves to be a more stable and effective additive under the testing conditions, sustaining lower wear rates and improved wear performance.

4.2. Results of Artificial Neural Network

The wear behavior is inherently influenced by several factors, including contact pressure, sliding velocity, material properties such as hardness and composition, and environmental factors like temperature[56] The ANN is particularly well-suited for modeling this complexity, as it learns nonlinear relationships between inputs and outputs by processing them through multiple layers and activation functions[57] In this study, we discuss the architecture, functionality, and advantages of an ANN designed to predict the wear coefficient $K\text{wANN}_{(p,v,\,c,\,H)}$. A four-layer neural network model was developed to estimate the COF and specific wear rate. The ANN's five input parameters are contact pressure P, sliding velocity V, and material properties, including hardness and composition (MoS_2 and graphite). The synergetic effect of graphite and MoS_2 was not considered, as these composites were treated independently. Appendix 1 presents the numerical details of ANN Input, Experimental Output, and Predicted Output data. Each input serves as a neuron or node in the input layer (refer to Appendix 1), and the data flows through hidden layers, where non-linear transformations are applied using weights w, biases b, and activation functions. The ANN architecture for wear prediction involves three hidden layers, each with a distinct activation function to capture specific aspects of wear behavior.

Figure 6 provides an overview of the ANN architecture. The first hidden layer uses a sigmoid activation function, which is commonly applied in neural networks for its smooth, non-linear characteristics that map inputs within a 0–1 range, allowing the

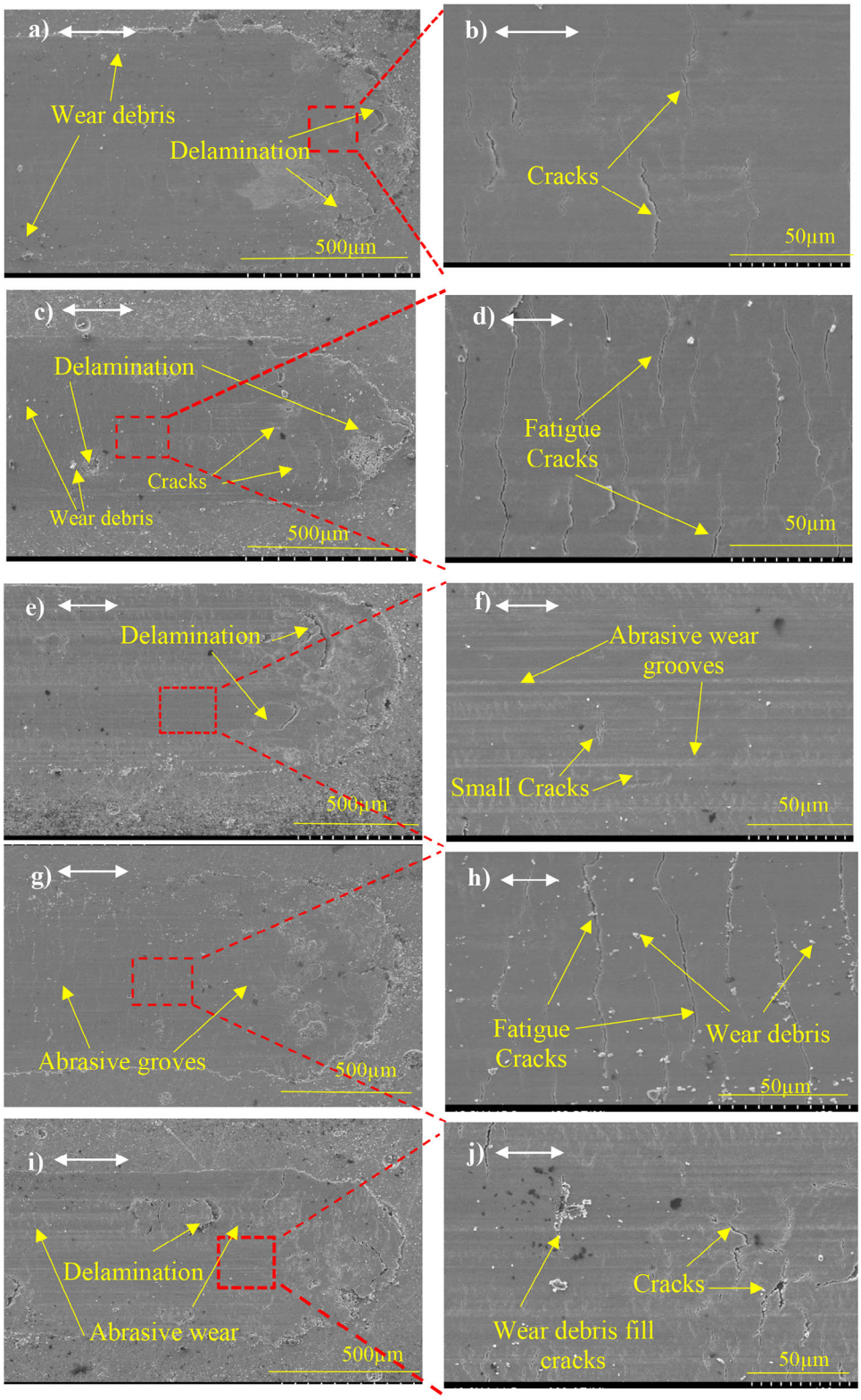

Figure 4. SEM images of 0.3 wt% graphite/epoxy composite wear track after 400 m sliding distance under different magnification. a,b) 10 N/2 Hz, c,d) 5 N/5 Hz, e,f) 10 N/5 Hz, g,h) 10 N/8 Hz, i,j) 15 N/5 Hz.

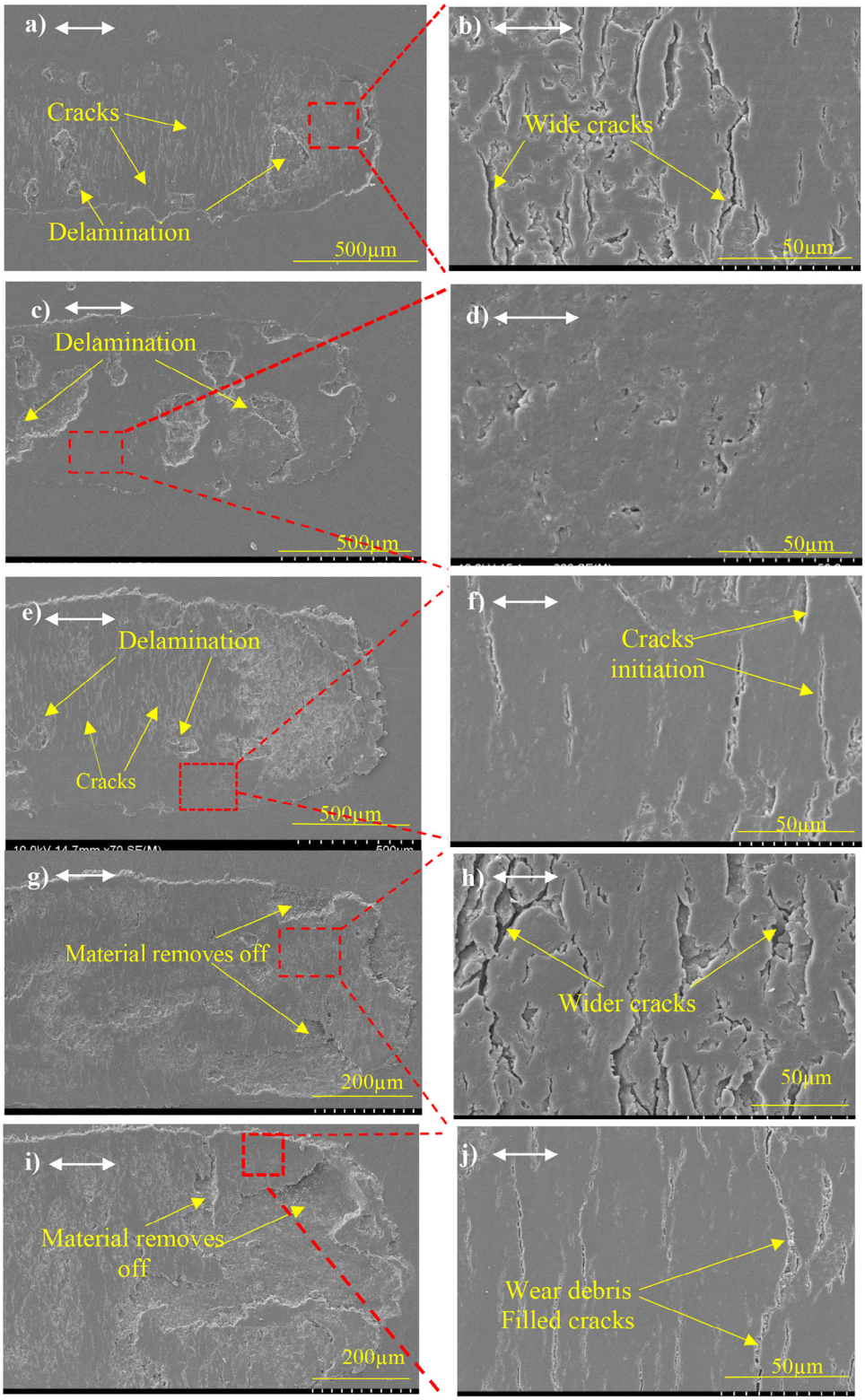

Figure 5. SEM images of 0.3 wt% MoS_2/epoxy composite wear track after 400 m sliding distance under different magnification. a,b) 10 N/2 Hz; c,d) 5 N/5 Hz; e,f) 10 N/8 Hz; g,h) 10 N/5 Hz, I,j) 15 N/5 Hz.

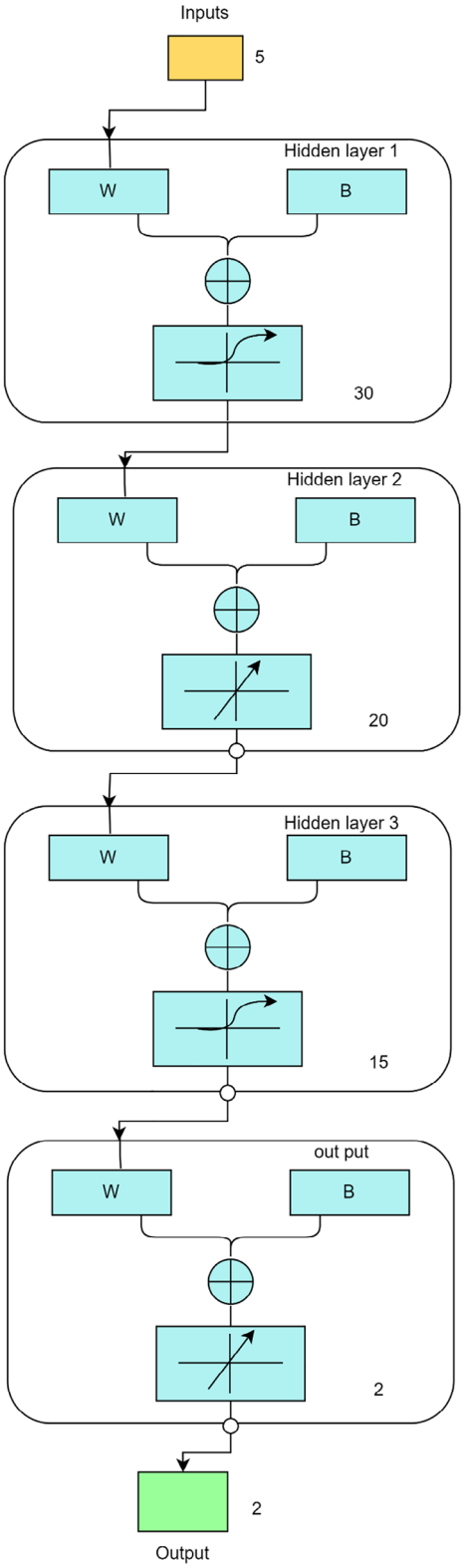

Figure 6. The general overview of the ANN architecture.

network to learn complex relationships between sliding velocity, contact pressure, and material behavior. This is crucial in tribology, where wear mechanisms often display non-linear relationships.

The second hidden layer employs a linear activation function that simply passes the weighted sum of inputs to the next layer, supporting the final prediction by combining complex patterns learned in previous layers. This linear layer aggregates the information into a continuous value representing the COF or specific wear rate.

To model power-law relationships frequently observed in tribology, such as wear rate dependence on pressure and velocity, a third hidden layer with a power activation function was implemented. Power-law relationships, like those in the Archard-Kragelsky wear law, exhibit a specific dependency on contact pressure and sliding velocity. The power activation function, expressed as power $(X) = X^n$ with n as a trainable exponent, enables the network to mimic these non-linear interactions, capturing the influence of pressure and velocity on wear rate. The output layer then provides the final prediction of wear behavior.

The ANN's degrees of freedom, or the total number of trainable parameters (weights and biases), were calculated based on the connections between the input, hidden, and output layers. Each neuron, excluding the input layer, has a bias, and each connection between neurons has an associated weight. For an ANN with four input neurons (representing pressure, velocity, hardness, and composition), hidden layers with ten, eight, and six neurons, and an output layer with three neurons (predicting COF and wear rate), the total degrees of freedom were determined by summing the weights and biases.

Figure 7 shows the neural network training regression. The data is divided into training (70%), validation (15%), and test (15%) sets, and the ANN is trained using backpropagation. The ANN model achieved a satisfactory fit to the experimental data. Balancing model complexity and available data is essential; adding neurons increases flexibility but can lead to overfitting if the training set is limited. Conversely, fewer neurons can reduce flexibility, leading to higher approximation errors. Consequently, the accuracy of the ANN model heavily relies on the quality and quantity of experimental data used in training. The coefficient of determination R^2 and MSE were used to evaluate model predictions for specific wear rate and COF.

Figure 8 presents regression plots evaluating the accuracy of specific wear rates and COF predictions for graphite/epoxy and MoS_2/epoxy composites. These plots encompass total model-predicted details outlined in Appendix 1. The network for predicting the wear rate has been performed using the entire data set of 50 experiments. Subfigures (a) and (b) depict the regression plots for the graphite/epoxy composite's SWR and COF, while (c) and (d) display those for the MoS_2/epoxy composite. The data in **Table 2** and Figure 8 give the comparative performance of the ANN models for tribological predictions of graphite and MoS_2 reinforced epoxy composites. The error validation results give a considerable difference in the predictive accuracy of the ANN model for graphite and MoS_2, based on the MSE and the R^2 metrics. For the COF, graphite predictions show a low MSE of 0.00073, indicating a minimal average error, and a high R^2 of 0.9047, meaning that over 90% of the variability in COF for graphite is accurately captured. This reflects a strong model fit

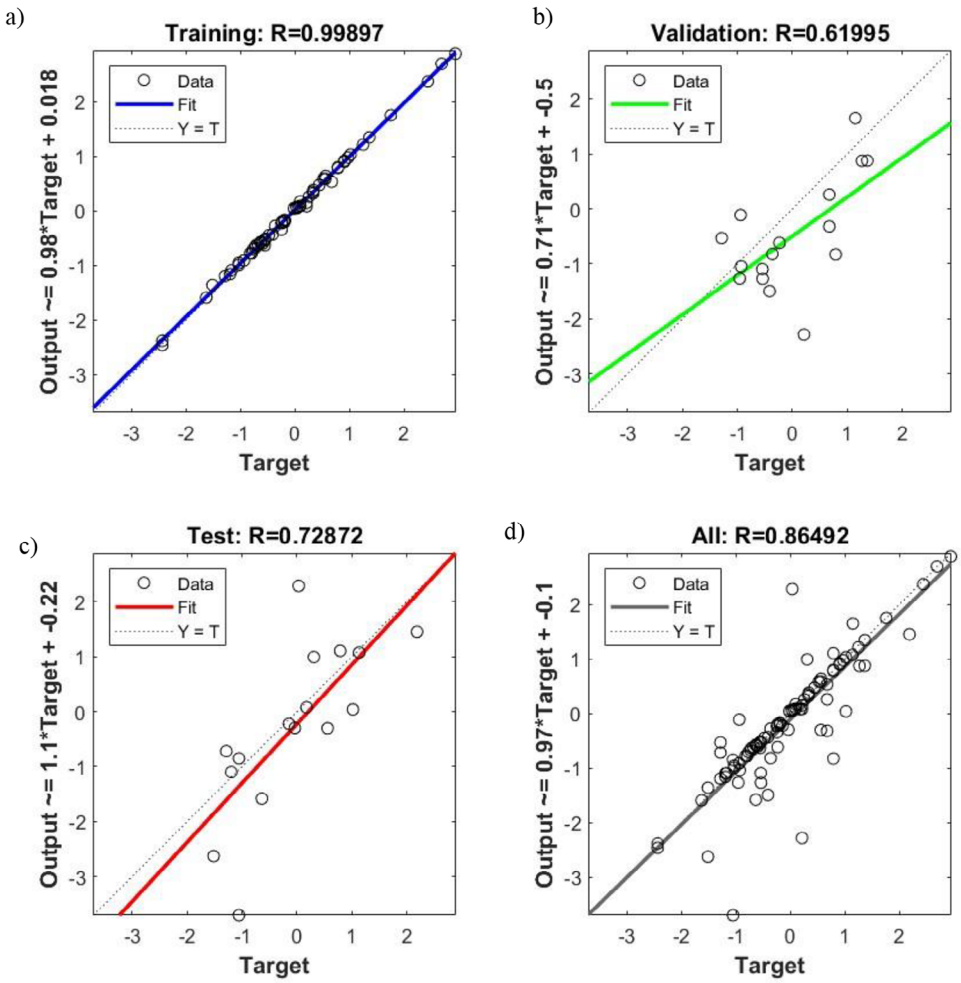

Figure 7. The neural network training regression a) training set, b) validation set, c) test, and d) network prediction set.

and high predictive accuracy for graphite. On the other hand, the model struggles with MoS_2, producing a MSE of 0.00318 and a lower R^2 of 0.5567. The lower R^2 value indicates that only a low percentage of the variability in COF is explained, revealing the model's limitations in accurately capturing the COF for MoS_2.

For specific wear rate predictions, graphite again outperforms MoS_2 in terms of model accuracy. The model achieves an MSE of 1.3351 and an R^2 of 0.9809 for graphite, showing very precise predictions with minimal error and almost all variability in wear rate captured by the model. Conversely, the MSE for MoS_2 rises to 1.6993, and the R^2 drops to 0.8271, indicating reduced accuracy compared to graphite, with higher prediction errors and a smaller portion of variability explained. These results collectively indicate that the ANN model is more effective for graphite, as the lower MSE and higher R^2 values demonstrate. The higher errors and reduced R^2 for MoS_2 suggest that the model has difficulty accurately capturing MoS_2's tribological behavior.

SEM observations provide insight into the discrepancies. Graphite-reinforced composites show less surface damage compared to MoS_2-reinforced composites, suggesting better wear resistance. This disparity, not fully captured in COF and SWR figures, indicates that graphite provides more stable protective properties under sliding conditions. MoS_2 lower prediction accuracy may stem from its susceptibility to oxidative degradation

Table 2. Summary of the ANN model prediction.

	Model prediction	Prediction for graphite	Prediction for MoS_2
MSE for COF	0.00195	0.00073	0.00318
R^2 for COF	0.7360	0.9047	0.5567
MSE for specific wear rate (SWR)	1.5172	1.3351	1.6993
R^2 for SWR	0.9726	0.9809	0.8271

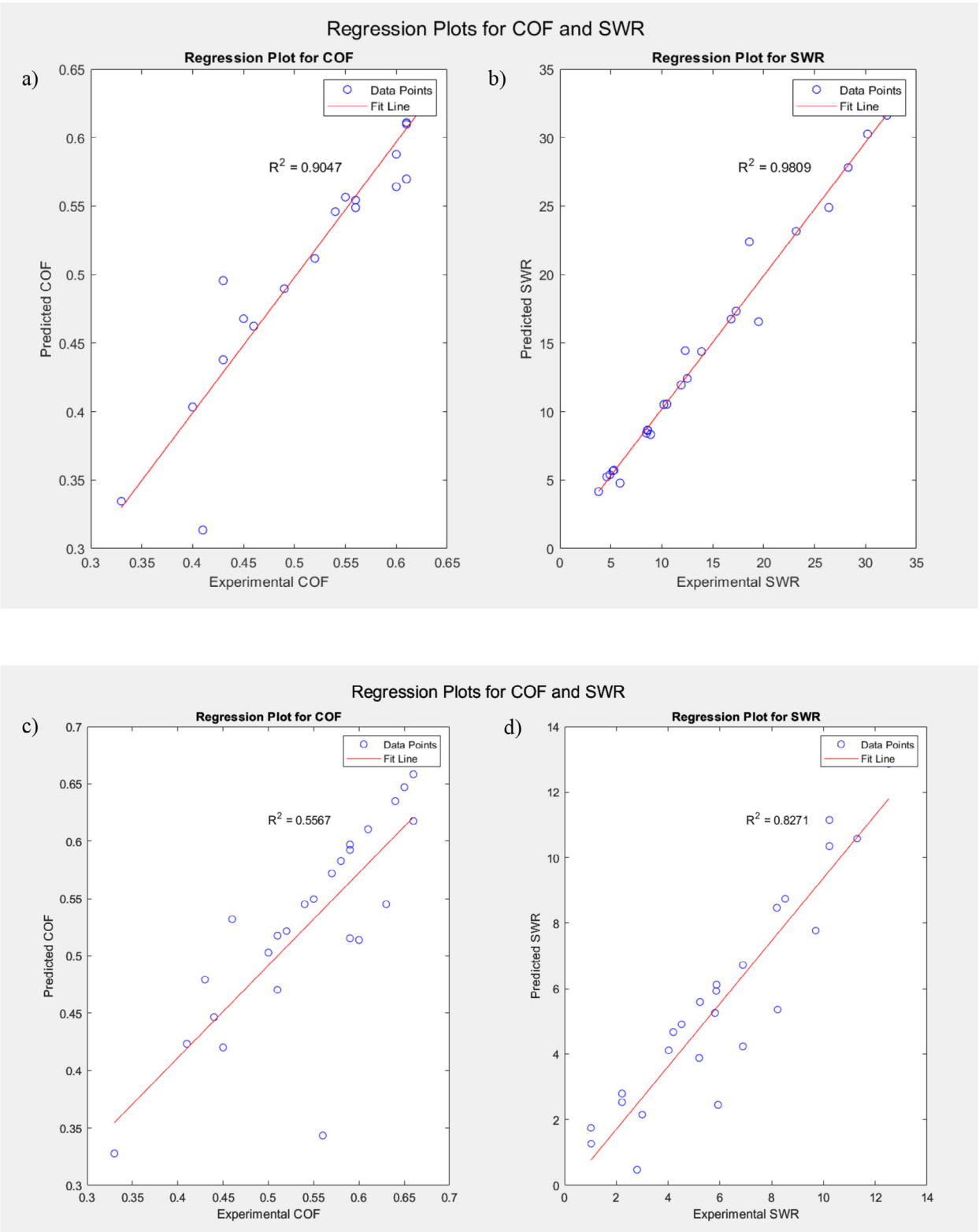

Figure 8. The regression plot of a) specific wear rate and b) COF of graphite/epoxy composite and the regression plot of c) specific wear rate and d) COF of MoS_2/epoxy composite.

in atmospheric conditions. When exposed to atmospheric oxygen and frictional heat, MoS_2 can form MoO_3, reducing its lubricating properties and wear resistance[55] However, the frictional heat generated during the sliding contact was not measured, which presents a limitation of this study. This omission may impact the understanding of the oxidative degradation behavior of MoS_2 under frictional conditions. This transformation complicates the material's tribological behavior, adding variability that the ANN struggles to predict accurately.

To further strengthen this idea, we perform XRD analysis on MoS_2 wear debris. Figure 9a is the SEM image of MoS_2 powder sample. This image provides a detailed surface morphology of the MoS_2 powder. The SEM visualization highlights the layered structure of MoS_2 particles, which is characteristic of its 2D lamellar morphology. Such a structure is crucial for its role as a solid lubricant. The XRD pattern of this MoS_2 powder sample is shown in Figure 9c. This pattern serves as a reference for comparison with the wear debris. It highlights the crystalline structure of pure MoS_2 before being incorporated into the composite or subjected to wear. Comparing this pattern with the wear debris can reveal if any degradation, oxidation, or phase transformation occurred during the sliding contact. **Figure 9b** is the XRD pattern that the crystalline phases present in the wear debris collected after subjecting the 0.3 wt% MoS_2 epoxy composite to a 15 N load, 5 Hz frequency, and 400m sliding distance against a chromium steel counterpart. During friction, MoS_2 is reduced to a few layers, resulting in sharper and more distinct peaks in the XRD pattern. In addition to peaks corresponding to MoS_2, some peaks indicative of MoO_3[58,59] can also be identified, suggesting possible oxidation of MoS_2 during the frictional contact. These observations provide valuable insights into the structural changes and tribological instability of MoS_2 within the composite matrix.

Graphite performs best in ambient and humid conditions with epoxy due to its enhanced interlayer slip from moisture adsorption, providing stable lubrication and thermal conductivity.[60–65] In contrast, MoS_2 excels under dry and vacuum environments and high load conditions, forming a robust tribofilm for effective lubrication but is susceptible to oxidation in ambient conditions.[55–58]

MoS_2 environmental sensitivity highlights the importance of including external conditions in ANN models for tribological applications. Variables like temperature, oxygen exposure, and humidity significantly affect wear mechanisms, particularly for materials prone to oxidative changes[55,66] Accounting for these environmental parameters could enhance ANN prediction accuracy by capturing the dynamic behavior of lubricating additives under varying conditions. Thus, while ANNs are effective for tribological predictions, considering environmental factors is crucial for robust predictions across composite systems.

We further explored the ANN's capability for tribological characterization by mapping surface plots. Using a trained ANN, the relationship between specific wear rate, contact pressure (P), and velocity (V) was examined. **Figure 10** depicts the impact of sliding velocity and pressure on the specific wear rate of a graphite–epoxy composite, showing a 3D surface plot and its bottom view of SWR variation with V and P. Similarly, **Figure 11** illustrates the same relationship for MoS_2 epoxy composites, indicating that wear rate may increase with higher pressures or velocities. Additionally, plots (c) and (d) in Figures 10 and 11 show COF variations under these conditions. These visualizations facilitate understanding of the combined effects of pressure and velocity on wear and friction, supporting the interpretation of tribological behavior.

The ANN model in this study, predicting COF and SWR for graphite- and MoS_2-reinforced epoxy composites, demonstrates varying accuracy compared to existing literature. For graphite/epoxy, the ANN achieves high precision (COF: MSE 0.00073, R^2 0.9047; SWR: MSE 1.3351, R^2 0.9809), surpassing the gradient boosting regression (GBR) model in a 2025 study on sericite/epoxy coatings, which reported COF and wear rate accuracies of 93.7% and 85.7%, respectively.[67] However, the ANN struggles with MoS_2/epoxy (COF: MSE 0.00318, R^2 0.5567; SWR: MSE 1.6993, R^2 0.8271), likely due to unmodeled oxidative degradation (MoS_2 to MoO_3). Literature reported that the MoS_2/SiC/epoxy composites, where a COF of 0.447 and wear rate of 14.39×10^{-5} mm^3 N^{-1} m^{-1} were achieved with 4 wt% MoS_2[68] that can be considered for future applications in the ANN. The ANN's predictive accuracy for MoS_2 is limited by environmental factors like humidity, unaccounted for in the model. A study on hemp fiber/epoxy composites using the Taguchi method identified time and speed as key wear influencers,[67] suggesting the ANN could improve by incorporating temporal dynamics. Lastly, a study on glass fiber/epoxy composites reported orientation-dependent wear rates (highest for AP-O fibers) under 30 N load,[69] indicating that fiber orientation, absent in the ANN inputs, could enhance prediction robustness. These comparisons highlight the ANN's strength for stable fillers like graphite but underscore the need to integrate environmental and structural variables for broader applicability.

Our study presents a significant advancement in predictive modeling for epoxy composites by simultaneously predicting both the COF and specific wear rate using an ANN. This dual-output approach contrasts with prior studies that primarily focused on single-output predictions limited to wear rate. Previous studies include models such as rice husk ash-reinforced aluminum alloy composites,[14] where parameters like sliding velocity, load, and reinforcement particle size were used to predict wear rate alone. Another approach applied the Archard-Kragelsky wear equation with a time-delayed neural network (TDNN)[52] for predicting wear rate during the running-in wear process for aluminum, achieving accuracy within 5%.

The superior predictive accuracy for graphite-reinforced composites was attributed to its stable tribological behavior and wear resistance, as confirmed by SEM observations. In contrast, MoS_2's tribological variability under ambient conditions contributed to reduced model accuracy. This novel dual-output predictive approach offers comprehensive insights into tribological performance and serves as a significant improvement over existing models limited to wear rate predictions.

5. Conclusions

This study used an ANN model combined with Kragelsky's friction law and Archard's wear law to predict the specific wear

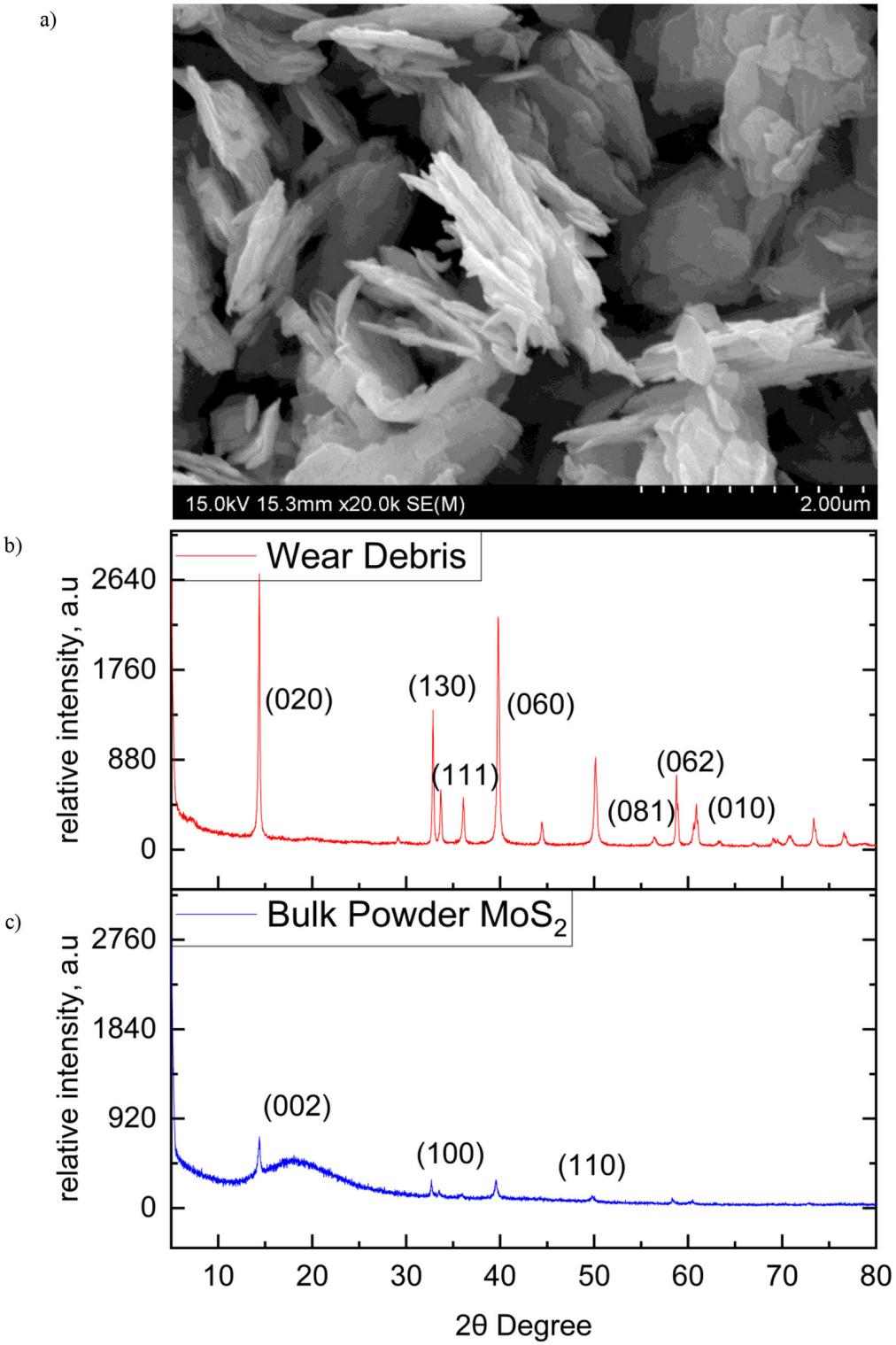

Figure 9. a) SEM image of MoS_2 powder sample, b) XRD pattern of wear debris collected from the 0.3 wt% MoS_2 epoxy composite after testing under 15 N load, 5 Hz frequency, and 400 m sliding distance against a chromium steel counterpart, and c) XRD pattern of MoS_2 powder.

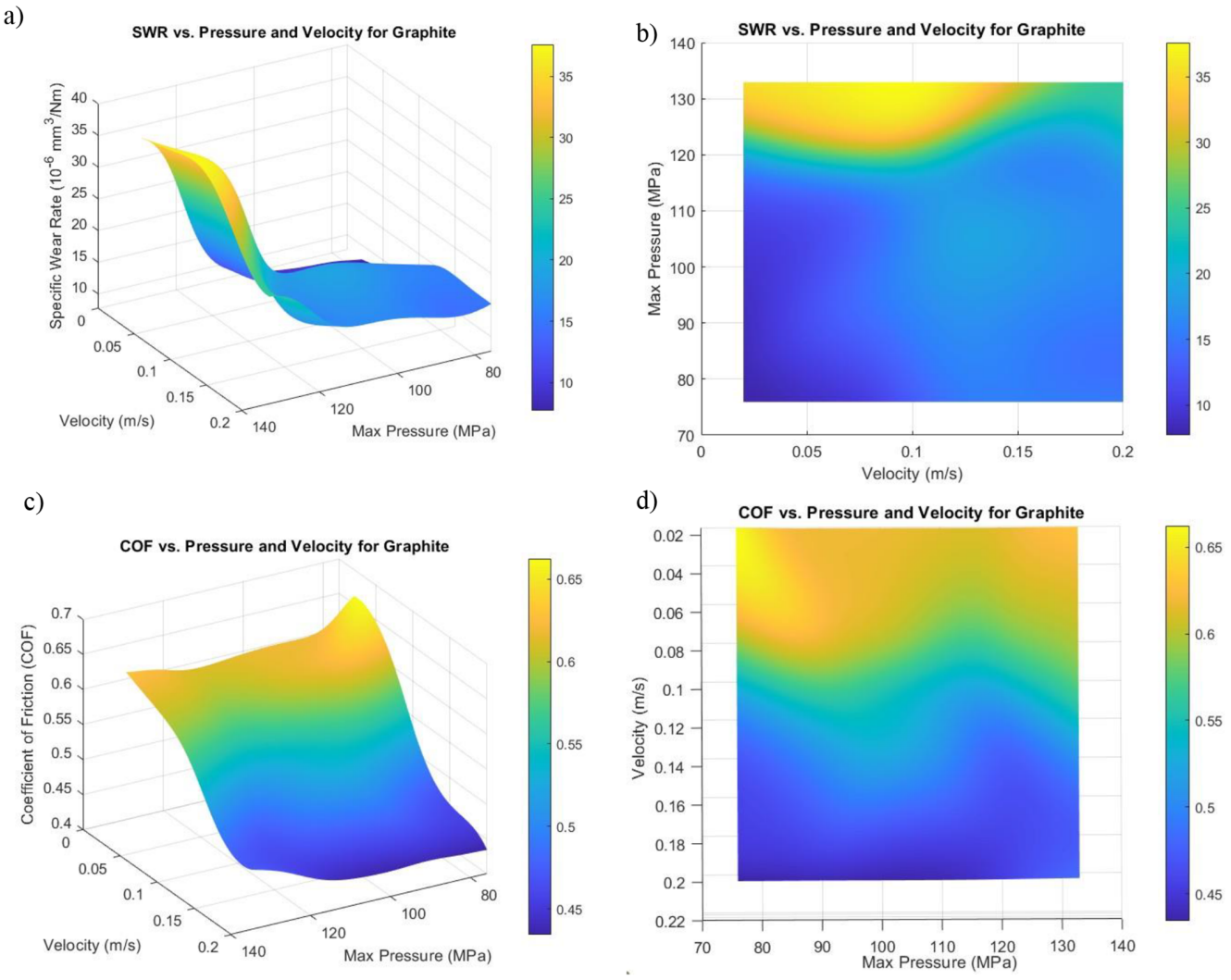

Figure 10. Graphite epoxy composite, variation of (*V*) with (*P*) with the specific wear rate a) 3D surface plot b) the bottom view of 3d plot and with the COF rate c) 3D surface plot d) the bottom view of 3d plot.

rate and COF in epoxy composites reinforced with graphite and MoS_2. The ANN's multi-layer architecture effectively captured the non-linear relationships among tribological parameters, including material properties, pressure, and velocity. Model performance was validated using experimental data, regression analysis, and MSE. The ANN achieved significantly higher prediction accuracy for graphite-reinforced composites compared to MoS_2. For the COF, graphite predictions yielded an MSE of 0.00073 and an R^2 of 0.9047, while MoS_2 predictions resulted in a higher MSE of 0.00318 and a lower R^2 of 0.5567. Similarly, for specific wear rate, graphite achieved an MSE of 1.3351 and an R^2 of 0.9809, whereas MoS_2 predictions showed a higher MSE of 1.6993 and a lower R^2 of 0.8271. SEM observations indicate that graphite provides greater wear resistance in epoxy composites compared to MoS_2.

This study presents a comprehensive response to developing a unified predictive model for epoxy composites containing graphite and MoS_2 as distinct lubricants. Graphite is a layered carbon structure with strong in-plane bonding and weak interlayer forces, making it an excellent solid lubricant even under ambient and humid conditions. MoS_2 is a layered transition metal dichalcogenide with a strong sulfur–metal–sulfur sandwich structure. Superior lubrication is available in dry and vacuum environments, but it is less effective on moisture compared to graphite. The challenge in developing a unified model lies in the different tribological behaviors of these lubricants, their tribofilm formation mechanisms, and their response to stress (load, speed) and environmental factors. To address these complexities, extensive experimental data were collected under varying pressure conditions, using multi-output models to predict wear and

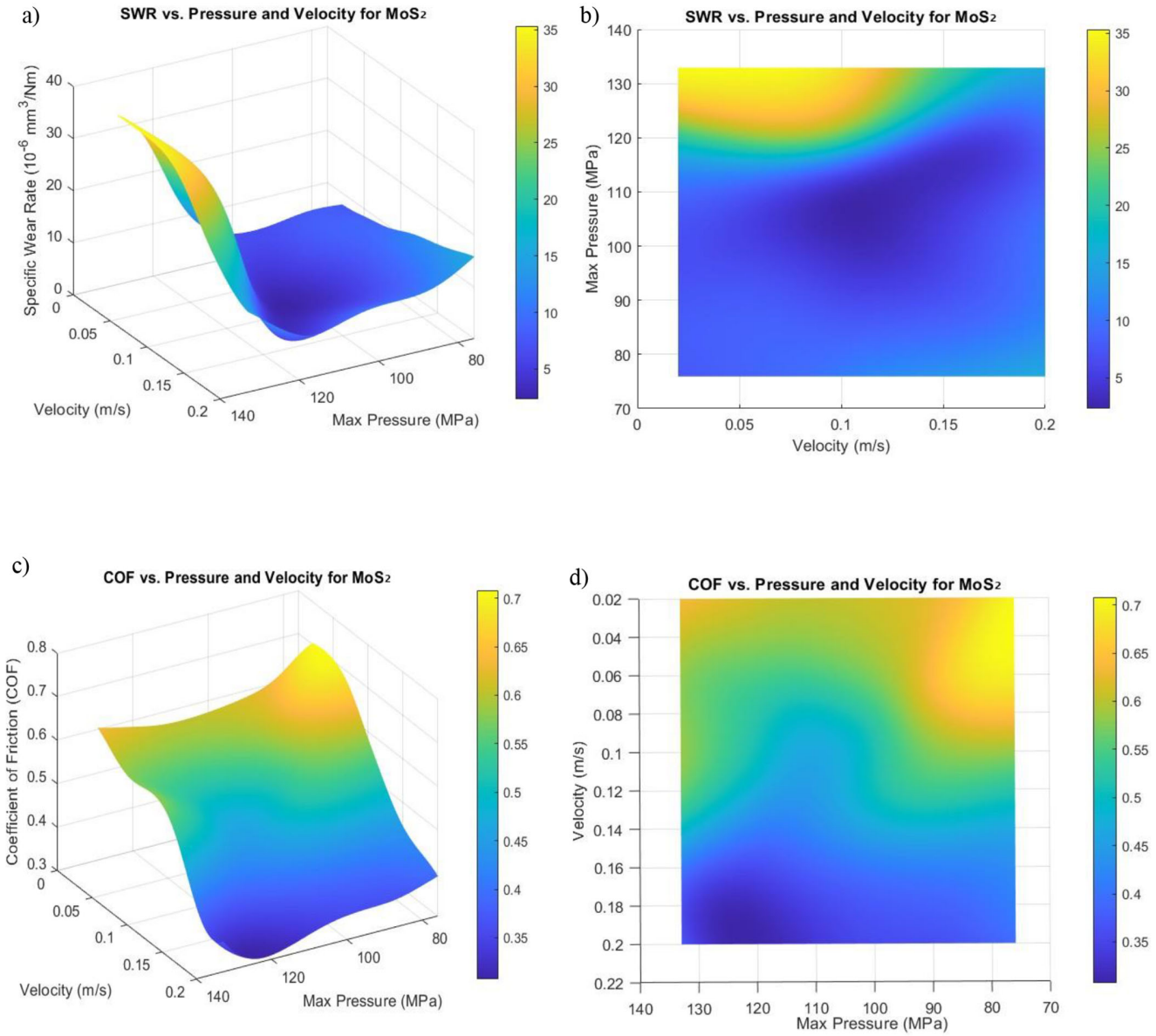

Figure 11. MoS_2 epoxy composite, variation of (*V*) with (*P*) with the specific wear rate a) 3D surface plot b) the bottom view of the 3D plot and with the COF rate c) 3D surface plot d) the bottom view of the 3D plot.

friction simultaneously. Activation functions were carefully selected to capture the specific contributions of each lubricant, and validation was conducted using experimental data for both single and mixed lubricant systems.

This study did not account for critical environmental factors such as atmospheric humidity, oxygen levels, and frictional heat generated during sliding contact, which could influence tribological performance and could be the reason for the low level of model accuracy for MoS_2.

MoS_2 is highly effective in vacuum conditions due to its stable layered structure and excellent lubricating properties. However, under ambient conditions, it becomes susceptible to oxidation, leading to the formation of MoO_3. This oxide layer has inferior lubrication properties, resulting in increased friction and wear, which introduces variability and compromises the accuracy of friction predictions. Maintaining controlled environmental conditions such as a vacuum throughout the experiment is cost-prohibitive and poses a limitation in this study. Additionally, we suggest that future work should explore compensatory modeling techniques to account for environmental variability.

Appendix 1: Experimental design and the ANN summary of data

Experimental design					ANN input					Experimental output		Output predicted			
Epoxy	MoS_2 [wt%]	Graphite [wt%]	Load [N]	Frequency [Hz]	Graphite	MoS_2	Max. pressure [MPa]	Average velocity [m s^{-1}]	Hardness (Shore D)	COF	Specific wear rate ($\times 10^{-6}$ mm^3 N^{-1} m^{-1})	COF	Specific wear rate ($\times 10^{-6}$ mm^3 N^{-1} m^{-1})	Error COF	Error S.W.R
99.9	0.1	0	5	5	0.1	0	87.28	0.07	71	0.61	8.9	0.637563	8.324003	−0.02756	0.575997
99.9	0.1	0	10	2	0.1	0	107.89	0.02	71	0.62	8.6	0.620666	8.611871	−0.00067	−0.01187
99.9	0.1	0	10	5	0.1	0	108.55	0.07	71	0.61	12.5	0.61087	12.40817	−0.00087	0.09183
99.9	0.1	0	10	8	0.1	0	109.97	0.2	71	0.61	19.5	0.569799	16.55844	0.040201	2.94156
99.9	0.1	0	15	5	0.1	0	125.88	0.07	71	0.62	32.1	0.620163	31.63988	−0.00016	0.46012
99.8	0.2	0	5	5	0.2	0	82.29	0.07	80	0.6	5.3	0.587818	5.715821	0.012182	−0.41582
99.8	0.2	0	10	2	0.2	0	99.98	0.02	80	0.6	5.9	0.564147	4.782384	0.035853	1.117616
99.8	0.2	0	10	5	0.2	0	99.98	0.07	80	0.54	10.2	0.545852	10.50976	−0.00585	−0.30976
99.8	0.2	0	10	8	0.2	0	103.68	0.2	80	0.4	17.3	0.403325	17.32005	−0.00332	−0.02005
99.8	0.2	0	15	5	0.2	0	118.68	0.07	80	0.55	28.3	0.556466	27.81214	−0.00647	0.48786
99.7	0.3	0	5	5	0.3	0	76.5	0.07	93	0.52	3.8	0.511676	4.154544	0.008324	−0.35454
99.7	0.3	0	10	2	0.3	0	98.83	0.02	93	0.49	5.2	0.489648	5.662616	0.000352	−0.46262
99.7	0.3	0	10	5	0.3	0	98.45	0.07	93	0.46	13.9	0.462244	14.37943	−0.00224	−0.47943
99.7	0.3	0	10	8	0.3	0	96.38	0.2	93	0.33	16.8	0.334454	16.74036	−0.00445	0.05964
99.7	0.3	0	15	5	0.3	0	110.33	0.07	93	0.45	26.4	0.467728	24.89667	−0.01773	1.50333
99.6	0.4	0	5	5	0.4	0	87.16	0.07	77	0.56	4.9	0.548929	5.385366	0.011071	−0.48537
99.6	0.4	0	10	2	0.4	0	106.49	0.02	77	0.56	4.6	0.554359	5.232637	0.005641	−0.63264
99.6	0.4	0	10	5	0.4	0	110.04	0.07	77	0.43	8.5	0.437767	8.425358	−0.00777	0.074642
99.6	0.4	0	10	8	0.4	0	109.82	0.2	77	0.41	12.3	0.313519	14.44385	0.096481	−2.14385
99.6	0.4	0	15	5	0.4	0	125.71	0.07	77	0.43	18.6	0.49551	22.38596	−0.06551	−3.78596
99.5	0.5	0	5	5	0.5	0	91.86	0.07	48	0.63	10.5	0.631162	10.53782	−0.00116	−0.03782
99.5	0.5	0	10	2	0.5	0	115.74	0.02	48	0.63	8.6	0.63129	8.656621	−0.00129	−0.05662
99.5	0.5	0	10	5	0.5	0	117.74	0.07	48	0.61	11.9	0.610975	11.9357	−0.00098	−0.0357
99.5	0.5	0	10	8	0.5	0	115.74	0.2	48	0.61	23.2	0.609734	23.16028	0.000266	0.03972
99.5	0.5	0	15	5	0.5	0	132.49	0.07	48	0.62	30.2	0.62112	30.25984	−0.00112	−0.05984
99.9	0	0.1	5	5	0	0.1	85.27	0.07	75	0.59	10.23	0.597033	10.34942	−0.00703	−0.11942
99.9	0	0.1	10	2	0	0.1	104.89	0.02	75	0.64	11.3	0.634952	10.57964	0.005048	0.72036
99.9	0	0.1	10	5	0	0.1	111.4	0.07	75	0.63	9.7	0.545058	7.770191	0.084942	1.929809
99.9	0	0.1	10	8	0	0.1	104.42	0.2	75	0.56	8.23	0.343316	5.363206	0.216684	2.866794
99.9	0	0.1	15	5	0	0.1	124.5	0.07	75	0.59	10.23	0.515333	11.15139	0.074667	−0.92139
99.8	0	0.2	5	5	0	0.2	81.65	0.07	85	0.61	12.52	0.610357	12.85785	−0.00036	−0.33785
99.8	0	0.2	10	2	0	0.2	99.89	0.02	85	0.54	5.23	0.545029	5.594613	−0.00503	−0.36461
99.8	0	0.2	10	5	0	0.2	99.49	0.07	85	0.58	5.87	0.582705	6.121578	−0.00271	−0.25158
99.8	0	0.2	10	8	0	0.2	102.97	0.2	85	0.45	5.2	0.420223	3.88296	0.029777	1.31704
99.8	0	0.2	15	5	0	0.2	119.04	0.07	85	0.5	8.52	0.502808	8.74286	−0.00281	−0.22286
99.7	0	0.3	5	5	0	0.3	75.93	0.07	88	0.52	2.22	0.521671	2.532769	−0.00167	−0.31277
99.7	0	0.3	10	2	0	0.3	95.94	0.02	88	0.51	2.8	0.47041	0.4752	0.03959	2.3248
99.7	0	0.3	10	5	0	0.3	94.23	0.07	88	0.46	3	0.531926	2.155193	−0.07193	0.844807
99.7	0	0.3	10	8	0	0.3	93.6	0.2	88	0.33	1.03	0.327736	1.26724	0.002264	−0.23724
99.7	0	0.3	15	5	0	0.3	113.13	0.07	88	0.44	2.22	0.44661	2.800447	−0.00661	−0.58045
99.6	0	0.4	5	5	0	0.4	82.42	0.07	81	0.43	1.02	0.479295	1.748981	−0.0493	−0.72898
99.6	0	0.4	10	2	0	0.4	103.22	0.02	81	0.41	4.2	0.423252	4.676542	−0.01325	−0.47654
99.6	0	0.4	10	5	0	0.4	99.61	0.07	81	0.51	4.52	0.517531	4.913504	−0.00753	−0.3935
99.6	0	0.4	10	8	0	0.4	103.17	0.2	81	0.55	5.86	0.549505	5.928907	0.000495	−0.06891
99.6	0	0.4	15	5	0	0.4	117.53	0.07	81	0.57	4.02	0.571879	4.119439	−0.00188	−0.09944
99.5	0	0.5	5	5	0	0.5	91.86	0.07	76	0.6	6.89	0.513956	4.23966	0.086044	2.65034
99.5	0	0.5	10	2	0	0.5	118.7	0.02	76	0.65	5.81	0.647117	5.256028	0.002883	0.553972
99.5	0	0.5	10	5	0	0.5	117.95	0.07	76	0.66	5.93	0.617714	2.452103	0.042286	3.477897
99.5	0	0.5	10	8	0	0.5	116.72	0.2	76	0.66	8.2	0.658478	8.466988	0.001522	−0.26699
99.5	0	0.5	15	5	0	0.5	132.93	0.07	76	0.59	6.89	0.592486	6.722938	−0.00249	0.167062

Acknowledgements

Open access publishing facilitated by Auckland University of Technology, as part of the Wiley - Auckland University of Technology agreement via the Council of Australian University Librarians.

Conflict of Interest

The authors declare no conflict of interest.

Data Availability Statement

The data that support the findings of this study are available from the corresponding author upon reasonable request.

Keywords

Archard wear law, artificial neural network, Kragelsky friction model, self-lubricating composites

Received: November 28, 2024
Revised: April 5, 2025
Published online:

[1] J. F. Archard, *J. Appl. Phys.* **1953**, *24*, 981.
[2] I. Argatov, W. Tato, *Eur. J. Mech.-A/Solids* **2012**, *34*, 1.
[3] S. K. Sinha, B. J. Briscoe, Polymer Tribology, Imperial College Press, London **2009**. https://doi.org/10.1142/p560
[4] J. K. Lancaster, *Tribology* **1972**, *5*, 249.
[5] H. J. Zhang, Z. Z. Zhang, F. Guo, *Tribol. Trans.* **2011**, *54*, 417.
[6] I. Argatov, *Front. Mech. Eng* **2019**, *5*, 30.
[7] J. Jang, S. Chen, J. Wang, *J. Mech. Des.* **1997**, *119*, 153.
[8] B. Stojanović, S. Gajević, N. Kostić, S. Miladinović, A. Vencl, *Ind. Lubr. Tribol.* **2022**, *74*, 350.
[9] N. A. K. Fountas, J. D, N. Vaxevanidis, *Tribol. Mater.* **2024**, *3*, 44.
[10] J. Shi, B. Zhao, J. He, X. Lu, *Tribol. Int.* **2024**, *198*, 109874.
[11] A. S. P. Vencl, S. Klančnik, A. But, M. Vorkapić, M. Harničárová, B. Stojanović, *Lubricants* **2023**, *11*, 24.
[12] S. Sathiyamurthy, S. Saravanakumar, V. Vinoth, *J. Reinf. Plast. Compos.* **2024**. https://doi.org/10.1177/07316844241256421
[13] N. Yin, Z. Xing, K. He, Z. Zhang, *Friction* **2023**, *11*, 1.
[14] I. I. Argatov, Y. S. Chai, *Tribol. Int.* **2019**, *138*, 211.
[15] Z. Yuhong, H. Wenxin, *Commun. Nonlinear Sci. Numer. Simul.* **2009**, *14*, 2373.
[16] Z. Zhang, K. Friedrich, K. Velten, *Wear* **2002**, *252*, 668.
[17] Z. Zhang, K. Friedrich, *Compos. Sci. Technol.* **2003**, *63*, 2029.
[18] D. M. Korres, G. Anastopoulos, E. Lois, A. Alexandridis, H. Sarimveis, G. Bafas, *Fuel* **2002**, *81*, 1243.
[19] T. Özel, Y. Karpat, *Int. J. Mach. Tools Manuf.* **2005**, *45*, 467.
[20] K. V. Rao, B. S. N. Murthy, N. M. Rao, *Measurement* **2014**, *51*, 63.
[21] A. Kumar, A. Mukhopadhyay, *Proc. Inst. Mech. Eng., Part E* **2024**, *238*, 723.
[22] D. Li, R. Lv, G. Si, Y. You, *Polym. Compos.* **2017**, *38*, 1705.
[23] Y. Ji, J. Bao, Y. Yin, C. Ma, *Recent Pat. Mech. Eng.* **2016**, *9*, 193.
[24] S. Sardar, S. Dey, D. Das, *J. Compos. Mater.* **2021**, *55*, 873.
[25] A. K. Kadiyala, J. Bijwe, *Wear* **2013**, *301*, 802.
[26] M. Z. Baltić, M. R. Vasić, M. D. Vorkapić, D. M. Bajić, J. Piteľ, P. Svoboda, A. Vencl, *Polymers* **2024**, *16*, 2976.
[27] L. M. Akuwueke, C. V. Ossia, H. U. Nwosu, *Tribol. Mater.* **2024**, *3*, 150.
[28] R. Joshi, P. K. Bajpai, S. Mukhopadhyay, *Biomass Convers. Biorefin.* **2024**, 1. https://doi.org/10.1007/s13399-024-06011-4
[29] I. O. Oladele, A. D. Akinwekomi, O. G. Agbabiaka, M. O. Oladejo, *J. Polym. Res.* **2019**, *26*, 1.
[30] P. Naik, P. Sahoo, S. K. Acharya, S. Pradhan, *J. Indian Acad. Wood Sci.* **2021**, *18*, 1.
[31] M. Alajmi, A. Shalwan, *Materials* **2015**, *8*, 4162.
[32] R. R. Jayasinghe, M. A. Nand, M. Ramezani, *Nanomaterials* **2024**, *14*, 1744.
[33] J. Smoleń, P. Olesik, K. Stępień, M. Mikuśkiewicz, H. Myalska-Głowacka, M. Kozioł, M. Godzierz, *Materials* **2024**, *17*, 1308.
[34] A. Kovalev, Y. Tian, Y. Meng, *Friction* **2024**, *12*, 1235.
[35] S. Sharma, in *Tribology of Polymers, Polymer Composites, and Polymer Nanocomposites* (Eds: S. C. George, J. T. Haponiuk, S. Thomas, R. Reghunath, P. S. Sarath), Elsevier, Amsterdam **2023**, pp. 401–435.
[36] P. Nagachandrika, K. Sridharan, R. Sarathi, N. Yoshimura, *Int. J. Soc. Mater. Eng. Resour.* **2018**, *23*, 195.
[37] S. R. Madeshwaran, R. Jayaganthan, R. Velmurugan, N. K. Gupta, A. V. Manzhirov, *J. Phys.: Conf. Ser.* **2018**, *991*, 12054.
[38] M. Zhao, L. Liu, B. Zhang, M. Sun, X. Zhang, X. Zhang, L. Wang, *RSC Adv.* **2018**, *8*, 35170.
[39] K. Friedrich, *Adv. Ind. Eng. Polym. Res.* **2018**, *1*, 3.
[40] B. J. Briscoe, S. K. Sinha, in *Wear – Materials, Mechanisms and Practice* (Ed: G.W. Stachowiak), Wiley, New York **2005**, pp. 223–267.
[41] S. K. Ray, A. Banerjee, B. K. Bhangi, D. Pyne, B. Dutta, in *Tribology of Polymers, Polymer Composites, and Polymer Nanocomposites* (Eds: S. C. George, J. T. Haponiuk, S. Thomas, R. Reghunath, P. S. Sarath), Elsevier, Amsterdam **2023**, pp. 17–50.
[42] H. Unal, S. H. Yetgin, A. Kastan, K. Ermis, V. F. Unal, *Materialwiss. Werkstofftech.* **2023**, *54*, 1249.
[43] M. Atta, M. Megahed, D. Saber, *Neural Comput. Appl.* **2022**, *34*, 14373.
[44] A. Shalwan, F. M. Alajmi, N. Alajmi, *J. Mater. Sci. Chem. Eng.* **2022**, *10*, 19.
[45] J. de Souza, I. Nascimento, S. Moreira, S. Cavalcanti, J. Medeiros, in *Proceedings of the 21st Brazilian Congress of Mechanical Engineering*, Universidade Federal da Paraíba, João Pessoa – PB, Brasil, **2011**, pp. 24–28.
[46] S. K. Balijepalli, R. Donnini, S. Kaciulis, R. Montanari, A. Varone, in *Materials Science Forum*, Trans Tech Publications Ltd, Bäch SZ, Switzerland **2013**, pp. 183–188.
[47] P. K. Balguri, D. H. Samuel, U. Thumu, *Mater. Today: Proc.* **2021**, *44*, 346.
[48] A. Zmitrowicz, *J. Theor. Appl. Mech.* **2006**, *44*, 219.
[49] V. Popov, *Facta Univ., Ser.: Mech. Eng.* **2019**, *17*, 39.
[50] I. I. Argatov, X. Gómez, W. Tato, M. A. Urchegui, *Wear* **2011**, *271*, 2857.
[51] I. I. Argatov, X. Gómez, W. Tato, M. A. Urchegui, *Wear* **2011**, *271*, 2857.
[52] I. Argatov, X. Jin, *Tribol. Int.* **2023**, *178*, 108021.
[53] I. I. Argatov, Y. S. Chai, *Front. Mech. Eng.* **2022**, *8*, 905026.
[54] H. C. Meng, K. C. Ludema, *Wear* **1995**, *181*, 443.
[55] X. Li, Y. Gao, J. Xing, Y. Wang, L. Fang, *Wear* **2004**, *257*, 279.
[56] A. Rosenkranz, M. Marian, F. J. Profito, N. Aragon, R. Shah, *Lubricants* **2020**, *9*, 2.
[57] U. M. R. Paturi, S. Cheruku, N. S. Reddy, *Arch. Comput. Methods Eng* **2022**, *29*, 3109.
[58] Y.-A. S. Chen, M.-Y., C.-C. Ho, S.-W. Ye, I.-W. P. Chen, Y.-Y. Shih, Y.-F. Shen, Y.-W. Chen, *RSC Adv.* **2023**, *13*, 29847.
[59] A. S. Gowrisankar, K. Sureka, T. Selvaraju, *Ionics* **2024**, *30*, 457.
[60] R. K. Upadhyay, A. Kumar, *Tribol. Int.* **2019**, *130*, 106.
[61] C. G. Gao, Q. Guo, F. Zhao, T. Wang, B. Jim, B. Wetzel, G. Zhang, Q. Wang, *Tribol. Int.* **2016**, *95*, 333.

[62] J. O. Moleń, P. K. Stępień, M. Mikuśkiewicz, H. Myalska-Głowacka, M. Kozioł, A. Gawron, M. Godzierz, *Materials* **2024**, *17*, 1308.
[63] R. M. Baptista, A. F. Rodrigues, C. Figueiredo-Pina, M. Guedes, R. Marat-Mendes, *Theor. Appl. Fract. Mech.* **2016**, *85*, 113.
[64] G. G. Pan, Q. Guo, J. Ding, W. Zhang, X. Wang, *Tribol. Int.* **2010**, *43*, 1318.
[65] N. Kumar, B. P. A. George, H. Abrahamse, V. Parashar, J. C. Ngila, *Appl. Surf. Sci.* **2017**, *396*, 8.
[66] B. C. Windom, W. G. Sawyer, D. W. Hahn, *Tribol. Lett.* **2011**, *42*, 301.
[67] H. Yan, J. Tan, H. Chen, T. He, D. Zeng, L. Zhang, *Polymers* **2025**, *17*, 282.
[68] C. Zhang, Y. He, S. Zhang, C. Li, R. Gou, J. Zhang, D. Sun, *Colloids Surf., A* **2024**, *700*, 134785.
[69] M. Huzaifa, S. Zahoor, N. Akhtar, M. H. Abdullah, S. Haider, S. U. Khan, K. Alam, *J. Mater. Res. Technol.* **2024**, *33*, 2785.